Science of Sintering, **50** (2018) 299-312

doi: https://doi.org/10.2298/SOS1803299T

UDK 666.3.019; 622.785

Microstructure and Phase Composition Of Steatite Ceramics Sintered by Traditional and Spark Plasma Sintering

Anja Terzić[1*)], Nina Obradović[2], Vaclav Pouchly[3], Jovica Stojanović[4], Karel Maca[3], Vladimir B. Pavlović[2]

[1]Institute for Testing of Materials IMS, Vojvode Mišića Bl. 43, 11000 Belgrade, Serbia
[2] Institute of Technical Sciences, Serbian Academy of Sciences and Arts, Knez Mihailova St. 35, 11000 Belgrade, Serbia
[3]CEITEC BUT, Brno University of Technology, Technicka 10, 61600 Brno, Czech Republic
[4]Institute for Technology of Nuclear and other Mineral Raw Materials, Franchet d'Esperey 86, 11000 Belgrade, Serbia

Abstract:

The influence of the sintering method on the mineral phase transformations and development of the crystalline microstructure of steatite ceramics was investigated. The steatite samples were fabricated from talc and bentonite as low-cost raw materials. Feldspar and barium carbonate, as fluxing agents, were altered in the steatite composition. Dilatometric analysis was applied in the monitoring of the dimensional changes and thereby densification of steatite during the traditional sintering (TS) procedure up to 1200 ℃. Spark plasma sintering (SPS) method was used under the following sintering conditions: 100 ℃/min heating rate, uniaxial pressure of 50 MPa; sintering temperature 800 °C/1 min or 1000 ℃/2 min. Crystallinity changes and mineral phase transition during sintering were observed by X-ray diffraction technique. Microstructural visualization of the samples and the spatial arrangements of individual chemical elements were achieved via scanning electron microscopy equipped with the EDS mapping. It was found that SPS sintering facilitated all microstructural changes during high temperature treatment and shifted them to lower temperatures. SPS treatment conducted at 1000 ℃ resulted in maximum densification of the steatite powder compacts and the formation stabilized protoenstatite structure.

Keywords: *Dilatometry; Spark Plasma Sintering; Electron microscopy; X-ray analysis; Microstructure-final; Magnesium silicate.*

1. Introduction

The ceramic products are commonly systematized as either construction or functional materials [1]. This classification is predominantly determined by the characteristics of a ceramic material in question. The behavior of the final ceramic output is also in direct correlation with the selection of raw materials for its production. Besides clayey binder and flux, the composition of silicate ceramics includes filler: quartz, alumina or magnesium silicate. The filler defines the performances of the product by being its predominant component [2, 3]. Thereby, the magnesium silicate based ceramics are mainly employed in the electrical engineering. The dielectric materials are produced by various processing schemes (e.g. dry pressing, extrusion, casting, semi-wet pressing), which all include sintering

*) **Corresponding author:** anja.terzic@institutims.rs

as the most important step [4, 5]. The sintering parameters and its route additionally shape the characteristics and the behavior of final ceramic product.

The steatite is a dielectric ceramic material with low dielectric loss, high mechanical strength, good electric properties and resistance to high temperatures [6, 7]. This material is a base for the manufacturing of insulators, regulator and bulb bases, switch parts, heating element holders, casings for thermostats, etc. [8–10]. The economical momentum is very important in the steatite production, because this material shows facilitated forming and relatively low sintering temperature [11]. The steatite, $Mg_3(Si_4O_{10})(OH)_2$, can be completely manufactured from natural raw materials, as the mineral base for its synthesis comprises talc and plastic clays [12]. The mixture of raw materials is fired at temperatures up to maximal 1400 °C depending on the selected sintering procedure [13, 14]. The mineral phases present in the steatite undergo crystallization, fusion and dissolution during the vitrification. The final steatite structure should resemble that of mineral enstatite as it comprises 70 % of crystalline $MgSiO_3$ (i.e. protoenstatite) and 30 % of glassy phase [15]. The development of microstructure and sintering behavior of steatite thereby depend on the ratio of formed crystalline and liquid phases [16–18]. The steatite's dielectric properties are strongly dependent on the temperature range and/or cycling (i.e. sintering regime) assigned for the given synthesis procedure [17]. Namely, since a complex series of polymorphic transitions take place in the steatite, this ceramic material can comprise four magnesium metasilicate forms: enstatite, protoenstatite, clinoenstatite, and high-temperature clinoenstatite [17, 18]. The thermodynamically sTab. crystals of protoenstatite initially appear above 985 °C, but the well-ordered and fully sTab. protoenstatite is usually obtained upon heating up to 1300 °C [19, 20].

Even though steatite is a valuable dielectric material, very few studies researched its sintering related properties [14–20]. This investigation provides insight into sintering behavior of steatites based of natural raw materials, i.e. talc and bentonite. In this work, two methods were applied in production of steatite ceramics: traditional sintering (TS) and spark plasma sintering (SPS). TS means a conventional pressure-less sintering in air atmosphere. SPS is a method for powder processing which is characterized by application of pulsed direct electric current and uniaxial pressure during sintering enabling a high-speed compaction [21]. It is highly efficient and applicable in the production of nano-materials, composites, dense solid materials, electronic materials, and biomaterials [22–25]. The SPS method has several advantages that distinguish it from the traditional sintering methods such as hot pressing and sintering of pre-compacted Tab.ts. When thoroughly managed, SPS enables also considerable control of the densification process and thus the tailoring of material microstructure. Also, the benefit of this method is that rapid densification is acquired in the early and/or intermediate sintering stages, during which the density rapidly increases from 50 % to 90 % of the theoretical density [26]. Such high densification rates are not usually attained in the conventional sintering processes, and their influence on the course of phase transformations taking place in the material is not understood yet. The focus of the experiment was to reach the maximal density of steatite powders in shorter time intervals by altering fluxing agents and sintering methods and to study of the phase composition and microstructure of the ceramics obtained by TS and SPS.

2. Materials and methods

Two steatite mixtures (ST1 and ST2) were used in the experiment. Both steatites comprised talc from Bela Stena deposit, Serbia, in 80 % of total mixture mass. Bentonite from Jelenkovac deposit (Serbia) was used as a binder in 10 wt. %. Different fluxing agents, in 10 wt. % each, were used. Feldspar from Bujanovac deposit (Serbia) was utilized in the ST1 mixture, while barium carbonate (Acros Organics, India) was flux in the ST2 steatite. The

chemical compositions of steatite mixtures, obtained by the X-ray fluorescence analysis (ED 2000 XRF spectrophotometer, Oxford Instruments, UK), are presented in the Tab. I. Representative samples (100 g) were pulverized in a laboratory vibratory mill prior to the testing. The loss on ignition (LoI) was determined as a weight difference between 20 and 1000 °C.

The micronization of green steatite powders was conducted in an ultra-centrifugal mill (ZM-1, Retsch, Germany). The mill comprised a 300 ml working element with a high-alloyed stainless steel rotor (∅100 mm, 600 W) and a variable mesh size ring sieves. The exit sieve with a 120 μm mesh size and trapezoid holes was used. The analytical fineness of the powder was acquired through repeated fracturing and welding of the particles. The rotor velocity was adjusted at 20.000 rpm. The milling period was set at 30 min.

. The dilatometric analyses were carried out in a high temperature dilatometer (L75 Platinum edition, Linseis, Germany). The samples in the shape of prisms 4 x 4 x 10 mm were sintered up to 1200 °C using the heating rate of 10 °C/min and dwell time of 1 h at maximal temperature. The sintering shrinkage and the coefficient of thermal expansion (CTE) were evaluated according to the procedure described in [27].

Tab. I Chemical analysis of ST1 and ST2 green powders.

Oxide, %	ST1	ST2
SiO_2	57.90	54.70
K_2O	0.70	0.20
Na_2O	0.73	0.69
Fe_2O_3	0.70	0.43
CaO	0.55	0.61
MgO	26.00	25.80
Al_2O_3	5.00	4.90
LoI	8.42	12.67

The SPS procedure was carried out in vacuum in a spark plasma sintering apparatus (Dr. Sinter 2050, SPS Syntex Inc., Japan). A batch of 2 g of the as-received powder was loaded in a cylindrical graphite die with an inner diameter of 12 mm and sintered under a constant uniaxial pressure of 50 MPa. The temperature was regulated by a pyrometer focused on the hole drilled to the radial surface of the graphite die. Two temperature profiles were used: 1) heating rate 100 °C/min, sintering temperature 800 °C, 1 min holding time; 2) heating rate 100 °C/min, sintering temperature 1000 °C, 2 min holding time. The relative density was measured by Archimedes method (EN 623-2) taking 3.21 g/cm^3 as the theoretical density of mineral enstatite.

Mineralogical analyses were performed on the pulverized green and sintered samples by means of the X-ray powder diffraction technique (XRD). The XRD patterns were obtained on a Philips PW-1710 automated diffractometer using a Cu tube. The instrument operates at 40 kV and 30 mA. It is equipped with a slanted graphite monochromator and a scintillation counter. The intensities of the diffracted CuKα X-ray emission ($\lambda = 1.54178$ Å) were measured at the ambient temperature in the intervals 0.02 °2θ in the 2θ Bragg angle range from 4 to 65 °2θ, counting for 0.5 s. The slits for the steering of the primary and diffracted beams were fixed at 1 ° and 0.1 mm.

The microstructure of the samples was observed by scanning electron microscope (JEOL, JSM-6390 LV). Parts of the sintered Tab.ts, whose surface was not polished prior to the imaging, were used in the analysis. The samples were covered with an Au film to improve the conductivity during recording. Energy-dispersive X-ray spectroscopic (EDS) analysis was conducted at the selected points on the steatite samples.

3. Results and discussion

The changes in the phase composition and the crystallinity of the steatite powders that took place with the increase in the temperature and the alternation of the sintering method were monitored. The X-ray diffraction analyses of the green steatite powders ST1 and ST2 are given in the Fig. 1a, and 1b, respectively. The ST1 and ST2 initial powders comprised certain number of the same phases: enstatite (JCPDS 86-0430), quartz (JCPDS 46-1045), kaolinite (JCPDS 14-164), and minerals from the smectite group (JCPDS 13-0135). Small amounts of feldspar (JCPDS 83-1370) were detected only in the ST1 sample because this mineral was used as a fluxing agent in this composition. The most significant XRD reflections (Fig. 1a, b) were located near 10 ° and 30 °. These peaks correspond to enstatite. Enstatite ($Mg_2Si_2O_6$), which is the most abundant mineral phase, originates from the talc. Small quantities of quartz (SiO_2) originate from the binder, i.e. bentonite, as well as the smectite minerals.

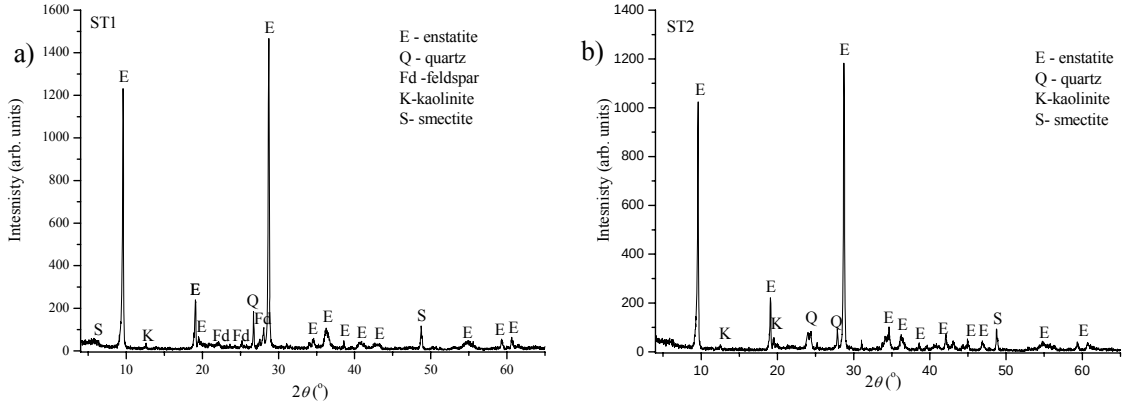

Fig. 1. The XRD diffractograms of the green steatite powders: a) ST1; and b) ST2.

The results of the X-ray diffraction analyses of the steatite powders ST1 and ST2 upon sintering in the dilatometer at 1200 °C are illustrated in the Fig. 2a, and 2b, respectively.

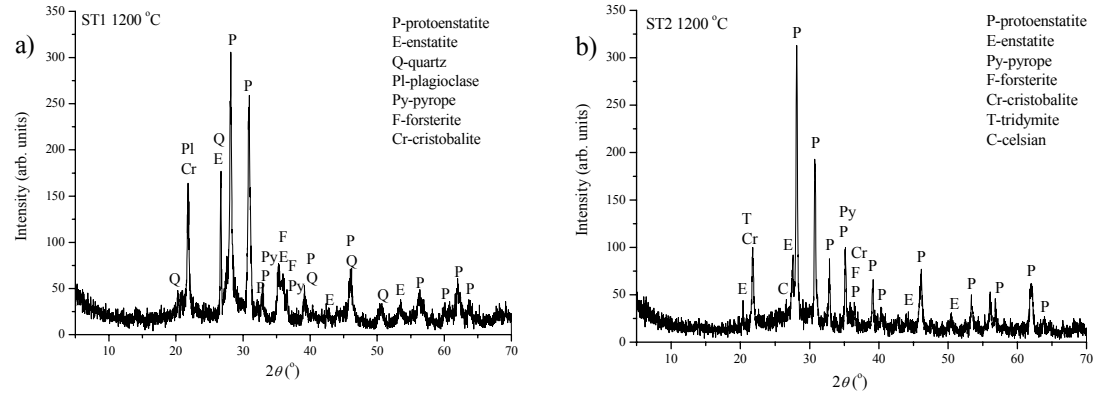

Fig. 2. The XRD diffractograms of steatite samples sintered via dilatometer at 1200 °C: a) ST1; and b) ST2.

The ST1 sample comprised the following mineral phases: P - protoenstatite (JCPDS 74-0816), E - enstatite (JCPDS 86-0430), Q - quartz (JCPDS 46-1045), Pl - plagioclase

(JCPDS 41-1480), Py - pyrope (JCPDS 15-0742), F - forsterite (JCPDS 34-0189), and Cr - cristobalite (JCPDS 82-0512). The minerals phases detected in the ST2 sample were: P - protoenstatite (JCPDS 74-0816), E - enstatite (JCPDS 86-0430), Py - pyrope (JCPDS 15-0742), F - forsterite (JCPDS 34-0189), Cr - cristobalite (JCPDS 82-0512), T - tridymite (JCPDS 42-1401), and C - celsian (JCPDS 38-1450). The high-temperature, sTab. polymorphic form of enstatite, i.e. protoenstatite, was the most abundant mineral phase registered in the diffractograms of both steatite samples. As showed in the investigations conducted by various authors [13, 17], enstatite mineral is subjected to a series of polymorphic transitions at elevated temperature. Namely, magnesium metasilicate can exist in four polymorphic forms, which are enstatite, protoenstatite, clinoenstatite, and high-temperature clinoenstatite. At the ambient temperature, magnesium metasilicate occurs in orthorhombic symmetry, as enstatite, which was proved by XRD analysis given in Fig. 1. Steady increase in the temperature up to approximately 1000 °C normally produces $Mg_2Si_2O_6$ polymorphs with an intermediate structure and an inversion tendency. STab. protoenstatite appears above 985 °C and gradually becomes the most dominant mineral phase in the 1000 °C to 1300 °C interval [17]. The XRD analyses given in Fig. 2 highlighted protoenstatite as the prevailing mineral phase in both ST1 and ST2 traditionally sintered samples. Quartz (SiO_2) as significantly less abundant phase was characterized by a very low crystallinity in the sample ST1. At 870 °C quartz ceases to be sTab. and, depending on the amount and type of the flux, it converts into cristobalite and/or tridymite. Thereby, cristobalite was registered in both steatite samples, while tridymite was present only in the ST2 sample. Since the peaks of quartz and its modifications were superposed both mutually and with the reflections of other mineral phases, their crystallinity could not be precisely detected. Other phases, such as pyrope ($Mg_3Al_2(SiO_4)_3$), forsterite (Mg_2SiO_4), and plagioclase were present in very small quantities. Plagioclase was detected in ST1 solely. Presence of plagioclase in this sample could be a result of the feldspar flux addition. Addition of barium carbonate flux in the composition of ST2 steatite resulted with presence of celsian ($BaAl_2Si_2O_8$).

The most significant reflections detected in the XRD diffractograms of ST1 and ST2 samples (Fig. 2a, and 2b) were located between 20 ° and 35 °. Two main peaks that correspond to protoenstatite were found at 28 ° and 32 °. The peaks at 28 ° were approximately the same in both samples as they counted up to 320 arbitrary units (a.u. in further text). The peak in ST1 sample, located at 32 °, was higher for approximately 70 a.u. The ST1 steatite showed a significant joint reflection of quartz and plagioclase at 22 °, while the diffractogram of the ST2 sample exhibited a smaller superposed peak of cristobalite and tridymite. The over-all crystallinity and the content of protoenstatite was approximately the same in both investigated steatite samples. The base lines of the diffractograms were not elevated, which refers to the presence of a relatively small amount of the amorphous phase.

The results of the X-ray diffraction analyses of the steatite powders ST1 and ST2 upon SPS sintering at 800 °C and 1000 °C are presented in the Fig.s 3a-d. The ST1 sample submitted to the SPS technique at 800 °C comprised three mineral phases: E - enstatite (JCPDS 86-0430), Q - quartz (JCPDS 46-1045), and Pl - plagioclase (JCPDS 41-1480). The minerals phases present in the ST2 sample that underwent the same sintering regime were: E - enstatite (JCPDS 86-0430), Q - quartz (JCPDS 46-1045) and W - witherite (JCPDS 44-1487). Protoenstatite was not yet formed in these samples after treatment at 800 °C, despite applied uniaxial pressure of 50 MPa. Plagioclase, detected in the ST1 sample, originates from feldspar. Detected witherite is a barium carbonate mineral, which belongs to the aragonite group. This mineral is characterized by orthorhombic symmetry. Witherite was found only in the ST2 sample due to the addition of $BaCO_3$ flux. The most significant XRD reflections that correspond to enstatite were located near 10 ° and 30 ° (Fig. 3a, and 3c), which are the same positions as in the green ST1 and ST2 samples. Intensity of the first peak located in the ST1 sample was reduced for 900 a.u. In the sample ST2 this difference was lesser: 500 a.u. The

second peak of the ST1 sample decreased for 800 a.u., while the change in the ST2 scaled down for 600 a.u.

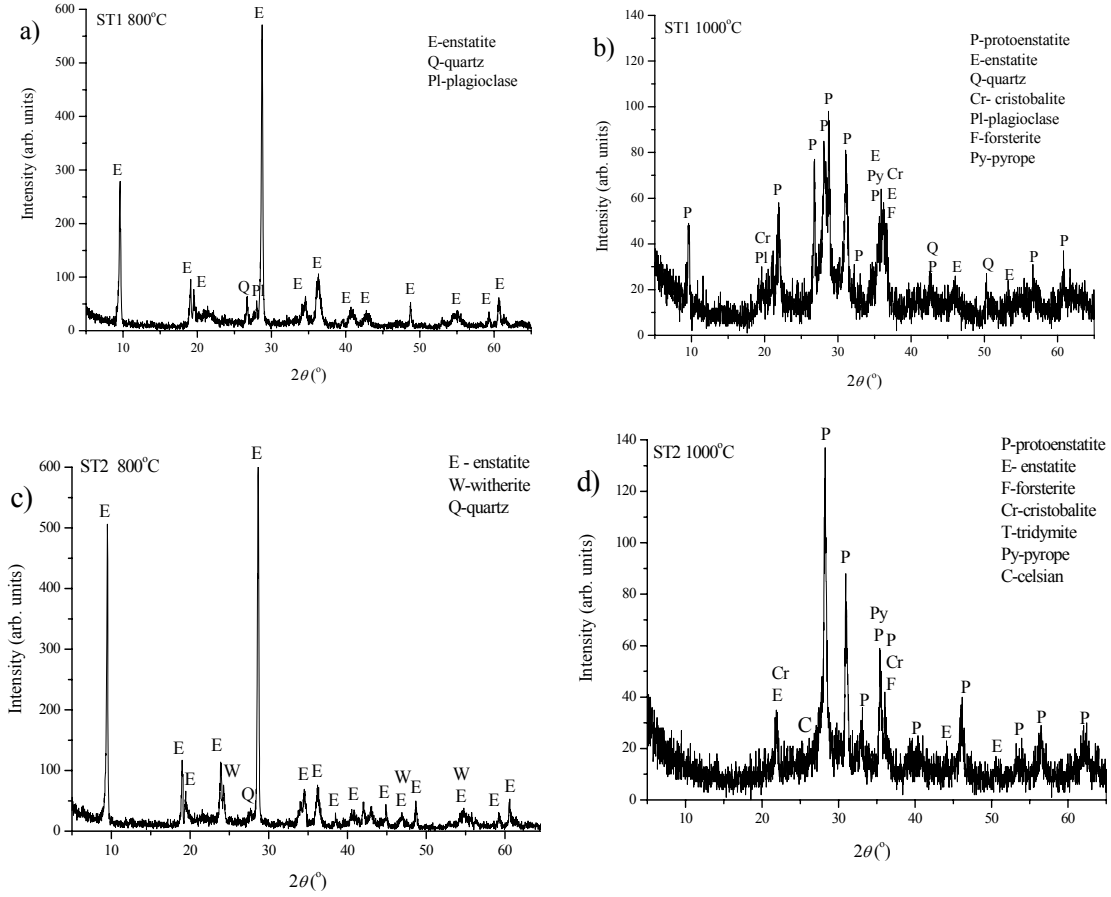

Fig. 3. The XRD diffractograms steatite samples treated via SPS: a) ST1 at 800 °C; b) ST1 at 1000 °C; c) ST2 at 800 °C; and d) ST2 at 1000 °C.

The SPS sintering conducted at 1000 °C and 50 MPa load produced certain changes in mineral phase composition of the steatite samples. Namely, the phases detected in the ST1 sample were: P- protoenstatite (JCPDS 74-0816), E - enstatite (JCPDS 86-0430), Q - quartz (JCPDS 46-1045), Pl - plagioclase (JCPDS 41-1480), Py - pyrope (JCPDS 15-0742), F - forsterite (JCPDS 34-0189), and Cr - cristobalite (JCPDS 82-0512). In the ST2 sample were registered the following mineral phases: P- protoenstatite (JCPDS 74-0816), E - enstatite (JCPDS 86-0430), Py - pyrope (JCPDS 15-0742), F - forsterite (JCPDS 34-0189), Cr - cristobalite (JCPDS 82-0512), T - tridymite (JCPDS 42-1401), and C - celsian (JCPDS 38-1450). The mineral composition found in the SPS treated samples qualitatively resembled the detected mineralogy of the traditionally sintered samples (Fig. 2a, and 2b). The acquired crystallinity of the samples submitted to the SPS sintered was lower than that of traditionally sintered samples probably due to the shorter sintering time and/or applied pressure. Also, the alternations in the applied flux resulted in the differences in the degree of crystallinity, thereby the ST1 sample exhibited lower crystallinity than sample ST2 after sintering at 1000 °C and 50 MPa pressure.

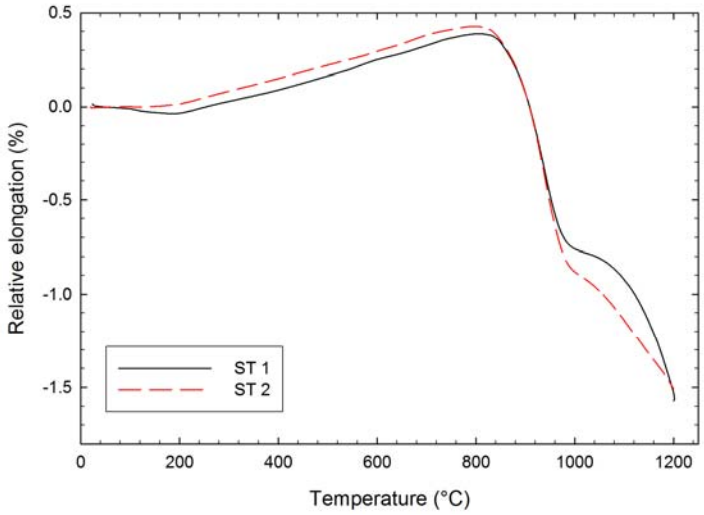

Fig. 4. Dilatometric curves of the ST1 and ST2 steatite samples.

The sintering behavior of steatites, with respect to the employment of different flux agents, was identified by monitoring of the dimensional changes of green steatite samples via dilatometric analysis and SPS technique; the acquired diagrams are presented in Fig.s 4 and 5, respectively. It should be noticed, that the thermally activated samples' length changes can be generally caused by superposition of the following phenomena: thermal dilatation, phase transformations, evaporation of volatile compounds, and sintering shrinkage. These changes can in some cases occur in simultaneously and therefore they cannot be easily separated. Anyway the temperature of significant changes in the dilatation curves can be a good indicator of the ongoing processes.

It can be seen from the Fig. 4 that the sample behavior up to 800°C can be described as a standard thermal dilatation with the coefficient of thermal expansion of CTE = $11 \cdot 10^{-6}$ K^{-1} (200-800°C). Since the steatite is primarily based on talc, its thermally induced behavior should be determined by the dehydration of talc mineral. Namely, talc incorporates adsorption water and hydroxyl groups situated in the space lattice elements [28]. In pure talc, water is normally eliminated in three stages: 115–200 °C; 350–500 °C, and 600–1050 °C [29]. In our case, the dilatation curves are evidently influenced in the first stage (up to 200°C), where the thermal dilatation of the sample was probably compensated by water evaporation.

The presence of quartz in the mineralogical composition alters the standard curve of talc's dehydration, because quartz undergoes a polymorphic transformation as its α–modification reversibly transforms into β–quartz at 573 °C [29, 30]. As it was showed by the XRD analysis (Fig. 1), the quantity of quartz is moderate and the resulting effects on the thermal curves are expected to be relatively small. Certain changes can be expected at 800 °C when the crystallization of magnesium metasilicate takes place as talc decomposes into magnesium oxide and silica due to the liberation of constitution water [28, 30]. The onset of shrinkage on the dilatometric curves at 800°C can be therefore addressed to crystallization magnesium metasilicate. Further decomposition of talc leads to the formation of protoenstatite (i.e. sTab. enstatite modification) and amorphous SiO_2. These changes are normally taking place at approximately 1100 °C, but 950 °C can be accepted as the initial temperature of sTab. enstatite formation [28, 30], which was indicated by the change in shrinkage rate at ca 1000 – 1050 °C in Fig. 4 . Also, the crystalline rearrangements that take place in the "in-between" thermal interval can be correlated with the reversible transition of enstatite from low-clinoenstatite to high-clinoenstatite [29]. A well-ordered crystalline structure in which protoenstatite is the predominant mineral phase as the sTab. enstatite polymorph is

established at 1200 °C. This is supported by the results of the XRD analyses (Fig. 2), which showed that protoenstatite comprises 90 % of all crystalline phases in each of the investigated samples.

The absence of thermal dilatation in the interval from 20 to 200 °C in the dilatometric diagram of both samples indicates the water dehydratation. The curve registered for ST1 sample showed a higher dehydratation than for sample ST2. This interval corresponds to the first dehydration stage of talc. Afterwards, the ST1 and ST2 diagrams showed an increasing trend up to 800 °C, which is caused by thermal dilatation of the samples. The shrinkage of the ST1 steatite sample registered in the interval from 800 to 1000 °C was 1.2 % and was probably caused by superposition of sintering shrinkage and magnesium metasilicate formation. This thermal sequence is significant because its end marks the beginning of the enstatite transformation into its sTab. polymorph. ST1 sample underwent another dimensional change above 1000 °C. The measured displacement was 0.8 %, which made total displacement (measured above 800 °C) to count up to 2.0 %. The diagram of the ST2 sample was characterized by a similar steep shrinkage from 800 to 1200 °C, with the total displacement in this interval summing up to 1.9 %. The variations in the sintering behavior of the investigated steatites were induced by the utilization of different flux. The addition of feldspar induced a two-step dilatometric displacement in thermal interval from 800 to 1200 °C, while $BaCO_3$ addition generated a more continual dimensional change. The density measurements performed after sintering at 1200 °C for the period of 1 h showed that the ST1 sample acquired 81.2 % of what can be considered as theoretical density of the natural mineral enstatite (TD = 3.21 g/cm^3). The sample ST2 achieved 83.7 % of theoretical density under same conditions. The obtained densities were 2.61 g/cm^3 and 2.70 g/cm^3 for the samples ST1 and ST2, respectively.

The densification measurement performed after SPS sintering at 800 °C for the period of 1 min showed that the ST1 sample acquired 76.7 % (or 2.46 g/cm^3) of the theoretical density of enstatite. The sample ST2 achieved 83.0 % (or 2.69 g/cm^3) of theoretical density under same conditions.

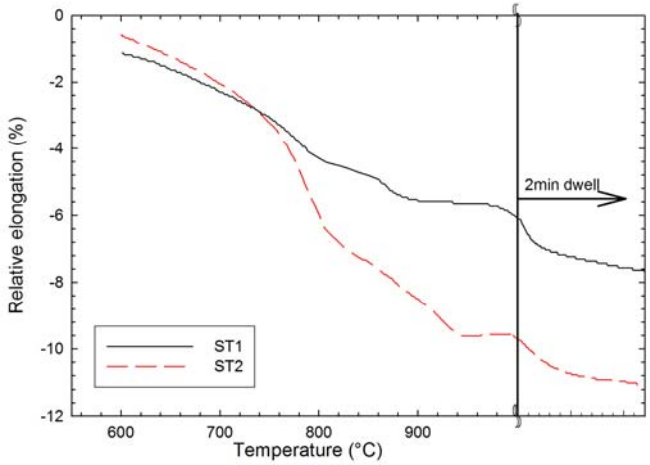

Fig. 5. Spark plasma sintering curves of steatite samples (1000 °C, 50 MPa, 2 min).

Fig. 5 shows the dilatation curves of samples ST1 and ST2 acquired by monitoring of the piston displacement in SPS during the experiments. It can be noticed that these elongation values can be hardly compared with that obtained from high temperature dilatometer, because the shrinkage in SPS is only one dimensional and SPS apparatus is not primarily designed for precise dilatometry. Anyway the temperatures of significant changes in dilatation curves are significant for the processes occurring during high temperature treatment..

It can be seen that, unlike in dilatometer, in SPS the sample shrinks from the beginning of the heating. This behavior can be attributed to the low temperature sliding of talc particles under the pressure of 50 MPa [26]. The faster shrinkage of both samples starts at ca 750 °C and we can assume that the same processes as during TS (sintering and magnesium metasilicate formation) occur but from slightly lower temperatures (750 °C during SPS vs. 800 °C during TS). The same was valid also for the second significant change in the slope of shrinkage curve – the formation of ensteatite starts in SPS at ca 960 - 990 °C while during TS this process started at ca 1000 - 1050 °C. The density measurements performed after SPS sintering at 1000 °C for the period of 2 min showed that the ST1 sample with the acquired 86.3 % (or 2.77 g/cm^3) and the ST2 sample with 94.1 % (or 3.02 g/cm^3) of the enstatite theoretical density have higher densities than those registered upon traditional sintering.

The SEM microstructural analysis was conducted on the parts of the crushed steatite samples which were previously sintered in the dilatometer at 1200 °C (Fig. 6) and the samples that were submitted to the SPS technique at 1000 °C (Fig. 7). The base material used in the steatite synthesis is talc, which indicates that the green steatite samples predominantly inherit its characteristic shell silicate structure with triclinic symmetry [10]. With the increasing sintering temperature, certain unfavorable microstructural changes can take place within the steatite structure: the formation of micropores that size up to 500 Å and the appearance of free SiO_2 (quartz) [10]. An applied sintering method should be able to reduce the microporosity characteristic for the talc grains and to prevent quartz recrystallization. Also, upon reaching of the protoenstatite stabilization form in the structure of steatite material, the sintering procedure should be able to induce the formation of a glassy matrix that additionally reinforces the new protoenstatite crystals. Acquiring of the described steatite "theoretical" microstructure guarantees the prevention from reversible phase transformations that would otherwise induce cracking and defects within the sintered ceramic.

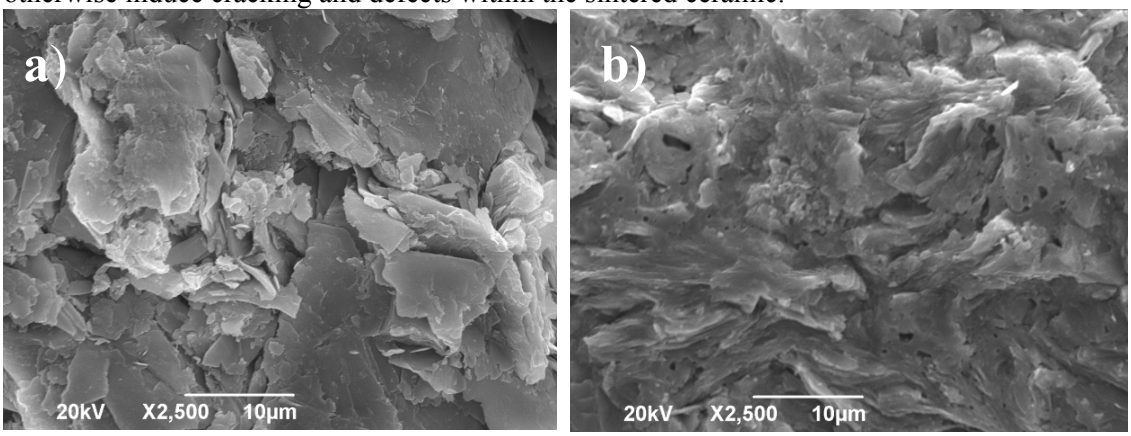

Fig. 6. The SEM microphotographs of the steatites sintered in the dilatometer at 1200 °C: a) ST1; and b) ST2.

The SEM microphotograph (Fig. 6 a) of the ST1 steatite sample obtained upon sintering at 1200 °C illustrates a mixture of differently shaped particles. The diameters of the particles are ranging in a wide interval from 2.19 μm to 24.63 μm. The recorded particles have different mineralogical origin: protoenstatite, enstatite, quartz, plagioclase, pyrope, forsterite, and cristobalite. However, the majority of the particles present at this temperature correspond to the mineral protoenstatite, as it was shown in the XRD diffractogram illustrated in Fig. 2 a. This sTab. enstatite polymorph is normally characterized by relative massive prismatic crystals with an average diameter of approximately 10 μm. This is in agreement with obtained dimensions of the recorded particles. Protoenstatite crystals also have a lamellar structure, which is recorded in the microphotograph. Very small, i.e. microcrystalline particles

normally correspond to quartz. Their quantity is small and they are distributed on the surfaces of the larger protoenstatite particles.

The ST2 steatite sample, which was submitted to the sintering via same method using same sintering parameters and temperature, showed a significantly more compact microstructure (Fig. 6 b). This sample comprised protoenstatite, enstatite, pyrope, forsterite, cristobalite, tridymite, and celsian. The present particles were comparatively smaller as their diameters ranged from 0.54 μm to 8.27 μm. Very small particles, with the diameters lesser than 1 μm, were merged and a consolidated with coarser grain structure during the sintering procedure. The smallest particles correspond to cristobalite and tridymite, while the large structures could be correlated with protoenstatite. Pores were also very small with an average diameter below 1 μm. Also, this sample contains a higher amount of the amorphous matter in comparison with ST1 steatite. The formation of additionally glassy substance that encircles and stabilizes protoenstatite crystals is enabled by utilization of $BaCO_3$ flux. The addition of barium carbonate flux contributed to the more compact structure, which is in agreement with obtained density values, i.e. higher density was obtained for the ST2 sample.

Since the densities of the steatite samples obtained in the SPS apparatus at 800 °C were as low as 76.7 % of TD, it can be assumed that at this point, the connections between particles are still weak, which would probably result in low physico-mechanical properties and unsatisfactory dielectric characteristics of the synthesized material. However, the ST1 sample recorded upon SPS treatment at 1000 °C (Fig. 7 a) showed relatively compact structure, as well as significant diversities in the comparison with the same steatite submitted to the traditional sintering.

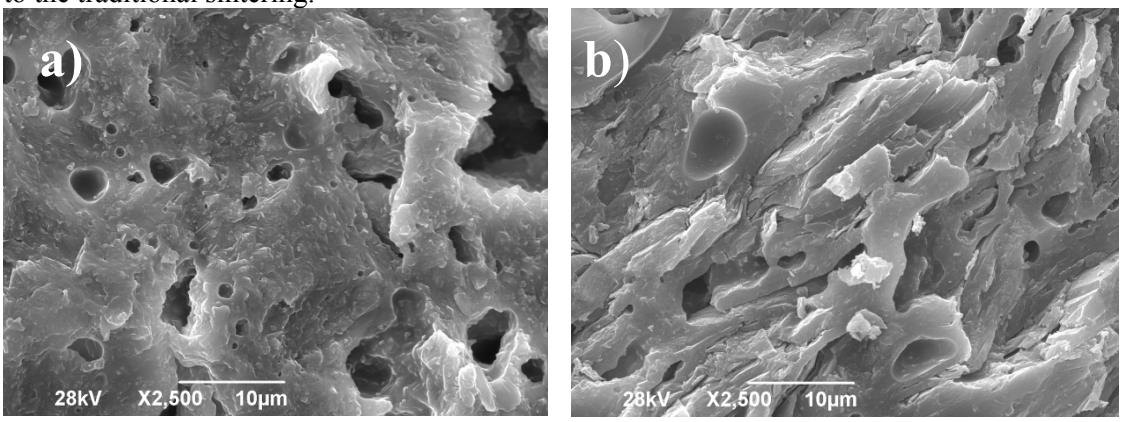

Fig. 7. The SEM microphotographs the steatites sintered in the SPS apparatus at 1000 °C: a) ST1; and b) ST2.

Most of the "coarse" particles merged forming what can be called a monolithic structure. The fine particles, visible on the surface of this structure, had really small dimensions (less than 3.46 μm). These small particles underwent additional consolidation with "coarser" grains during the sintering procedure and created strong bonds. According to the XRD analysis the majority of the particles are related to the mineral protoenstatite. Small particles can be correlated to either quartz (smaller spherical to rounded particles - spherulites) or its modification (platy to sheet forms or as pseudo-hexagonal crystals), but also plagioclase, forsterite or pyrope. The grain boundaries between large particles appear solid and strong. Also, the glassy phase, which was created due to application of high temperature and pressure, filled out the open pores present in the material and stabilized newly formed enstatite crystals, and thereby contributed to the fabrication of a dense sample with no signs of structural cracking. The sample ST2 (Fig. 7 b) showed even denser structure (94.1 % of TD) with all previously described positive characteristics of the ST1 steatite.

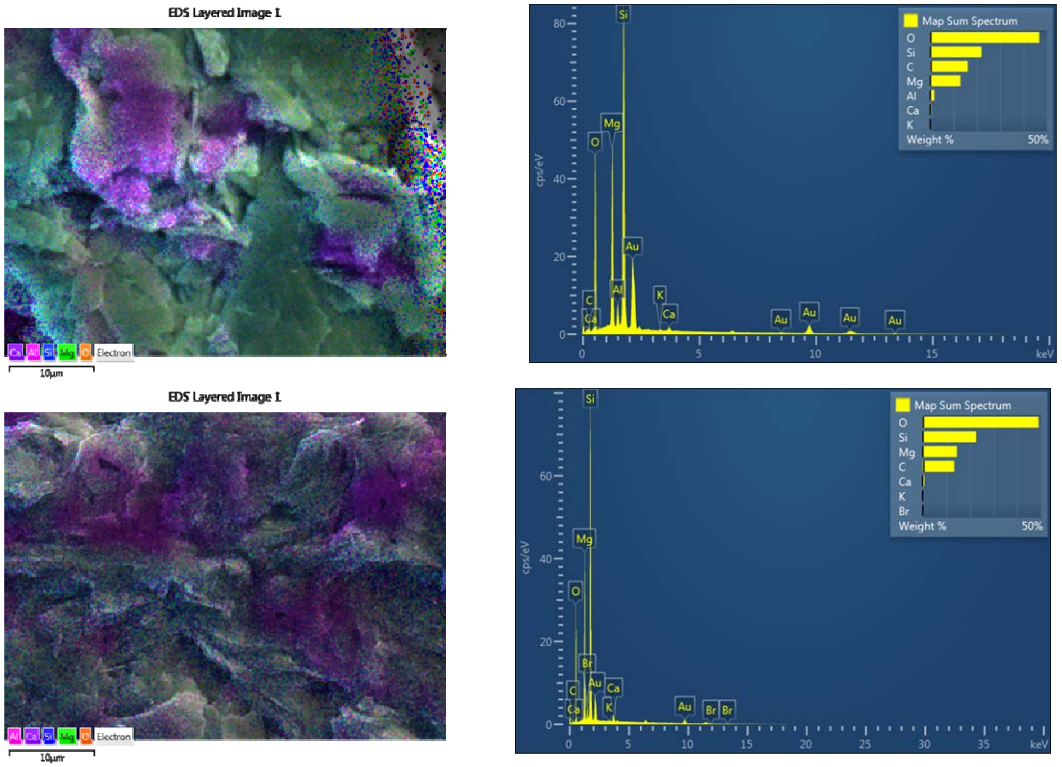

Fig. 8. EDS mapping (left), and elemental analyses (right) of the steatite samples from Fig. 6 a, and 6 b.

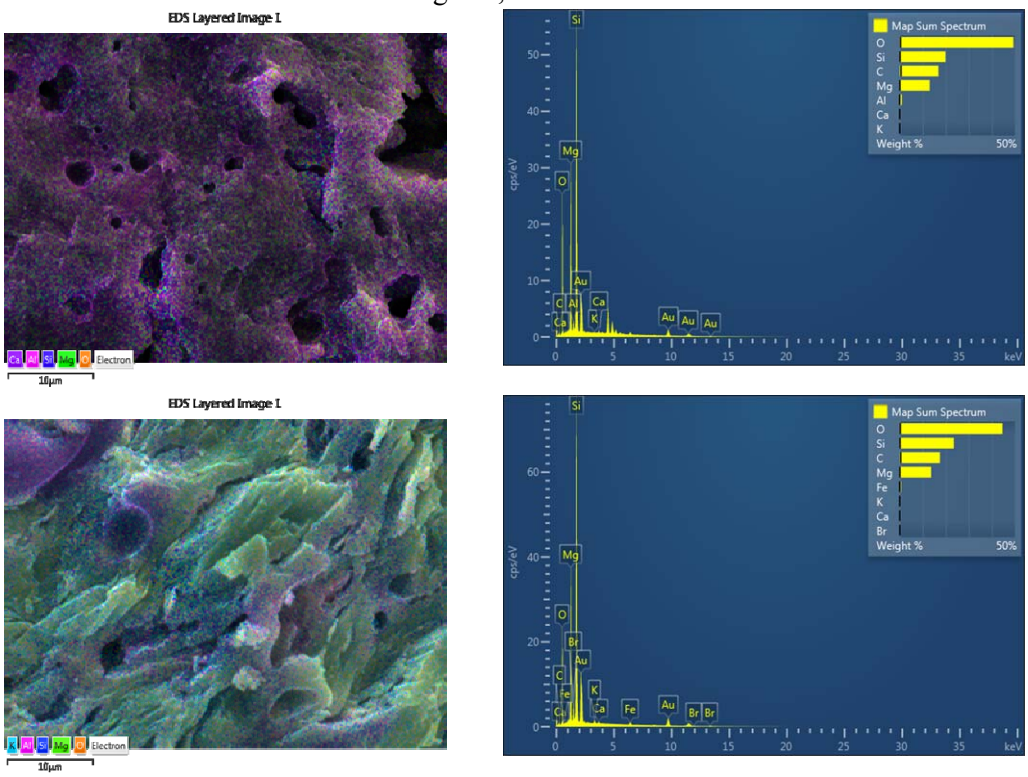

Fig. 9. EDS mapping (left), and elemental analyses (right) of the steatite samples from Fig. 7 a, and 7 b.

This means that by application of the SPS method a dense ceramic material with no signs of structural cracking or similar defects can be produced at a lower temperature (1000 °C) than that of traditional sintering (1200 °C).The EDS analyses of the SEM microphotographs (from Fig. 6, and 7) are given in Fig.s 8, and 9. The conveyed EDS analyses endorse the results of the chemical (Tab. I) and mineralogical (Fig. 2, 3 b, and 3 d) investigations of the ST1 and ST2 steatites. The most abundant chemical elements detected in all investigated samples were silicon (> 26.23 %) and magnesium (> 14.82 %). Si and Mg are chemically merged in magnesium silicate, i.e., one of the mineralogical modifications of talc (mineral enstatite). Aluminum is present in a small quantity 0.44–1.23 %, probably as Al_2O_3. The aluminum originates from the applied binder, i.e. bentonite. The percentage of elemental oxygen is around 40–50 %. The oxygen is present in the form of oxides. Potassium is present in very small amounts (< 1 %).

The EDS elemental mapping on the SEM images gave an insight into the spatial arrangements of individual chemical elements in the recorded steatite samples upon traditional sintering at 1200 °C and SPS treatment conducted at 1000 °C. Thereby, it can be seen that the majority of the element-related points on the microphotographs belong to Mg, Si, and O which originate from talc. Mg, Si, and O are homogenously distributed on all images, as they are constituents of the sTab. form of mineral enstatite, i.e. protoenstatite.

4. Conclusion

This investigation gave an insight to the interconnections of sintering procedure, microstructural changes and development of the crystalline phases of two steatite types fabricated from low-cost raw materials (talc and bentonite) in regard to different fluxing agents (feldspar and barium carbonate). The X-ray diffraction analyses highlighted the tendency of steatite mixtures for establishing of the protoenstatite mono-phase system during sintering. Namely, both applied sintering methods, i.e. traditional sintering and the spark plasma sintering, promoted the formation of a sTab. polymorph of enstatite – protoenstatite, as the main mineral phase. The quantity of remaining mineral phases present at maximal sintering temperatures summed up to approximately 10 % of total crystalline phases. The alternations of flux agents in composition of steatite ceramics resulted in their different crystallinity degrees: ST1 steatite with addition of feldspar exhibited higher crystallinity, and ST2 sample with $BaCO_3$ was characterized by presence amorphous matter in higher abundance. Also, SPS method initiated formation of the additional amount of glassy phase which was responsible for the development of more compact samples with improved density.

Maximal densification of the steatite samples took place at 1200 °C during traditional sintering. The acquired densities were 81.2 % and 83.7 % of mineral enstatite theoretical density, for ST1 and ST2, respectively. Spark plasma sintering produced steatite samples with even higher densities (86.3 % for ST1 and 94.1 % for ST2) at lower sintering temperature (1000 °C). The glassy matter created due to the applied high temperature and pressure during SPS procedure was responsible for the stabilization of newly formed protoenstatite crystals, the elimination of enstatite reversible reactions, as well as the steatite structure reinforcement which contributed to the prevention of cracking and deterioration and suitability of this material for advanced engineering applications.

Acknowledgements

This investigation was supported by the Serbian Ministry of Education, Science and Technological Development and it was conducted under the following projects: ON 172057 and III 45008. The authors acknowledge also the support of the Grant agency of Czech

Republic under grant no. 17-05620S and support of the Ministry of Education, Youth and Sports of the Czech Republic under the project CEITEC 2020 (LQ1601).

5. References

1. W. Carty, U. Senapati, Journal of American Ceramic Society 81 (1) (1998) 3.
2. E. Vela, M. Peiteado, F. Garcia, A. Caballero, Ceramic International 33 (2007) 1325.
3. J. Liebermann, American Ceramic Society Bulletin 82 (2) (2003) 39.
4. H. Soykan, Ceramic International 33 (2007) 911.
5. P. Rohana. Neufuss, J. Matejícek, J. Dubský, L. Prchlık,C. Holzgartner, Ceramic International 30 (2004) 597.
6. A. Terzić**,** Lj. Andrić, J. Stojanović, N. Obradović, M. Kostović, Science of Sintering 46 (2) (2014) 247.
7. M. Valaškov, J.Zdrálková, J.Tokarský, G. Martynková, M. Ritz, S. Študentová, Ceramic International 40 (2014) 15717.
8. L. Munoz, S. Cava, C. Paskocimas, Ceramica 48 (308) (2002) 217.
9. V. Karayannis, A. Moutsatsou, E. Katsika, Science of Sintering 48 (2016) 363.
10. M. Chmielewski, K.Pietrzak, A. Strojny-Nędza, K. Kaszyca, R. Zyba, P.Bazarnik, M. Lewandowska, S. Nosewicz, Science of Sintering 49 (2017) 11.
11. W. Lee, A. Heuer, Journal of American Ceramic Society 70 (1987) 349.
12. J.V. Smith, Acta Crystallographica 12 (1959) 515.
13. J. Jiao, X. Liu, W. Gao, C. Wang, H. Feng, X. Zhao, L. Chen, Material Research Bulletin 45 (2010) 181.
14. Z.Yumei, Z. Fenglin, L.Pengcheng, B. Kun, W. Shanghua, L. Shaoming, Science of Sintering,
    49 (2017) 311.
15. B. Reynard, J.D. Bass, J.M. Jackson, Journal of European Ceramic Society 28 (2008) 2459.
16. M.D. Rigterink, Journal of American Ceramic Society 30 (7) (1947) 214.
17. P. Ptácek, K. Lang, F. Soukal, T. Opravil, E. Bartonícková, L. Tvrdík, Journal of European Ceramic Society (2014) 515.
18. H. Thurnauer, A.R. Rodriguez, Notes on the constitution of steatite, Journal of American Ceramic Society 25 (15) (1942) 443.
19. W.L. Brown, N. Moromoto, J.W. Smith, Journal of Geology 69 (1961) 609.
20. G.A. Rankin, H.E. Merwin, American Journal of Science (4th series) 45 (1918) 301.
21. M. Tribaudino, American Mineralogist 85 (2000) 707.
22. A. Goel, D. Tulyaganov, S.Agathopoulos, M. Ribeiro, J. Fereirra, Ceramic International 33 (2007)1481.
23. V. Tyrpekl, M. Holzhäuser, H. Hein, J. Vigier, J. Somers, P. Svora, Journal of Nuclear Materials 454 (2014) 398.
24. V. Chuvildeev, M. Boldinn, A. Nokhrin, A. Popov, Acta Astronautica 135 (2017) 192.
25. M. Koller, T. Chráska, J. Cinert, O. Heczko, J. Kopeček, M. Landa, R. Mušálek, M. Rameš, H. Seiner, J. Stráský, M. Janeček, Materials & Design 126 (2017) 351.
26. B. Obadele, O. Ige, P. Olubambi, Journal of Alloys and Compounds 710 (2017) 825.
27. D. Weller, D. Morelli, Journal of Alloys and Compounds 710 (2017) 794.
28. L. Wang, V. Pouchly, K. Maca, Z. Shen, Y. Xionga, Journal of Asian Ceramic Societies 3 (2015) 183.
29. K. Maca, V. Pouchly, A. Boccaccini, Science of Sintering, 40 (2008) 117.
30. M. Wesolowski, Thermochimica Acta 78 (1984) 395.
31. A. Terzić, L. Pezo, Lj. Andrić, M. Arsenović, Composites Part. B: Engineering 79

(2015) 660.
32. A. Wiewiora, S. Sanchez-Soto, M. Avilos, A. Justo, L. Perez-Maqueda, J. Perez-Rodriguez, P. Bylina, Applied Clay Science 12 (1997) 233.

Садржај: *Проучаван је утицај начина синтеровање на трансформације у минералном саставу и развој кристалне микроструктуре стеатитне керамике. Стеатитни узорци су справљени на бази талка и бентонита, који су економичне минералне сировине. У саставу стеатите варирани су топитељи – фелдспат и баријум карбонат. Димензионалне промене, а посредно и дензификација стеатита су праћени у току методе традиционалног синтеровања (ТС) помоћу дилатомтријске анализе до 1200ºC. Метода спарк плазма синтеровања је примењена под следећим условима: 100 ºC/min брзина загревања, једноаксијали притисак од 50 MPa; температуре синтеровања 800 °C/1 min или 1000 ºC/2 min. Промене у кристалиничности и минералним фазама у току синтеровања су праћени X-ray дифракционом техником. Микроструктурна визуелизација узорака и просторни распоред појединих хемијских елемената су праћени помоћу скенинг електронске микроскопије са EDS мапирањем. Откривено је да СПС синтеровање олакшава микроструктурне промене које настају при високо-температурном третману и помера их ка нижим температурама. СПС синтеровање резултирало је максималном дензификацијом компактираних стеатитних прахова и формирањем стабилне протоенстатитне структуре.*
Кључне речи: Дилатометрија; спарк плазма синтеривање; електронска микроскопија; X-ray анализа; финална микроструктура; магнезијум силикат.